Intergrain Coupling in Dusty-Plasma Coulomb Crystals

U. Mohideen,[1,*] H. U. Rahman,[2] M. A. Smith,[1] M. Rosenberg,[3] and D. A. Mendis[3]
[1]*Department of Physics, University of California, Riverside, California 92521*
[2]*IGPP, University of California, Riverside, California 92521*
[3]*Department of Electrical and Computer Engineering, University of California–San Diego, La Jolla, California 92093*
(Received 23 December 1997)

We have studied the lattice structure of dusty-plasma Coulomb crystals formed in rectangular conductive grooves as a function of plasma temperature and density. The crystal appears to be made of mutually repulsive columns of grains confined by the walls of the groove. The columns are oriented along the direction of the electrode sheath electric field. A simple phenomenological model wherein the intergrain spacing results from an attractive electric-field-induced dipole-dipole force balanced by a repulsive monopole Coulomb force is consistent with observed features of the Coulomb crystal. [S0031-9007(98)06620-4]

PACS numbers: 52.25.Vy, 52.65.Cc, 52.90.+z

A dusty plasma can be loosely defined as an ionized gas with dispersed charged solid particulates, or dust grains, of micron to submicron sizes. The physics of dusty plasmas in space environments, such as planetary atmospheres and rings, comets, and the interstellar and interplanetary media, have been studied for some time (e.g., [1–5]). Recently there has been much interest in the physics of dust in plasma processing devices, used in the microelectronics industry, primarily due to the defects in microelectronic circuits caused by dust contamination (e.g., [6,7]). Important new developments in laboratory dusty plasmas involve experiments demonstrating the formation of Coulomb lattices or crystals of charged dust grains in a plasma, the so-called "plasma crystals" [8–11]. As suggested by Ikezi [12], negatively charged dust grains (due to the higher mobility of the electrons) in a plasma can form Coulomb crystals when their Coulomb intergrain potential energy is sufficiently larger than their thermal energy. This condition is

$$\Gamma_d = \frac{e^2 Z_d^2}{dT_d} \exp(-d/\lambda_D) > \Gamma_{dc} ,$$

where Z_d is the dust charge state, d is the intergrain spacing, T_d is the dust grain thermal energy, λ_D is the plasma Debye length, and Γ_{dc} is some critical value which is approximately 170 for a one component plasma [12].

In Coulomb crystal experiments, the grains are confined in the sheaths of the electrode configurations. In the vertical direction the grains are levitated by the electrostatic force associated with the electric field in the sheath, while the monopole (Coulomb) repulsion between the grains keeps the spacings between the layers. In the horizontal direction, the grains are also confined by the force associated with the horizontal component of the electric field in the sheath. It has also been conjectured that there may be mechanisms which lead to additional attractive forces between the grains that may influence the lattice structure (e.g., [13–15]). Here we report on a new regime of dust Coulomb crystals, where the grain sizes are on the order of ~ 50 μm (larger than those in previous Coulomb crystal experiments), and where there appears to be a strong intergrain attractive coupling which leads to the formation of distinct grain columns along the sheath electric field. We attribute this to an electric-field-induced dipole-dipole interaction between the grains. This possibility has been proposed recently by an analysis of the phase diagram of such crystals [16]. We first give experimental results and then discuss our phenomenological model.

The experimental setup used at The University of California–Riverside (UCR) is shown in Fig. 1. A 10 cm diameter Pyrex four-way cross was used as the reaction chamber. Inside, 5 cm $\times$ 7.5 cm aluminum electrodes were arranged 5 cm apart in the form of a capacitor. The bottom electrode has a 1 cm deep, 4 cm wide, 7.5 cm long groove in the middle. The aluminum electrodes were coated with black conductive paint to minimize light scattering off the electrode. The front end of the groove was made of a conductive and transparent indium tin oxide (ITO) coated glass to facilitate easy observation of the Coulomb crystal from that direction. The rear end of the groove was capped with copper foil. A 100 turn 10 cm diameter Helmholtz coil is added to the chamber to generate a 50 G magnetic field which confines the plasma and leads to the efficient production of large particles during the growth process.

First the chamber was pumped below 1 mTorr and Ar gas was leaked into the chamber to a pressure of 60 mTorr. A 5 A current was then supplied to the Helmholtz coils. A stable plasma was next formed by supplying 15 W forward rf power at 34 MHz to the electrodes. SiH_4 and O_2 gases (about 20 mTorr of each) were then introduced into the chamber for 15 s and allowed to react. The reaction led to the nucleation of SiO_2 crystallites which grow in size by aggregation. The magnetic field was turned off at the end of the growth process (about 3 min) leading to a relatively homogeneous grain size distribution. Figure 2 is a scanning electron microscope image of a typical grain. The grains are porous aggregates of 100 nm sized

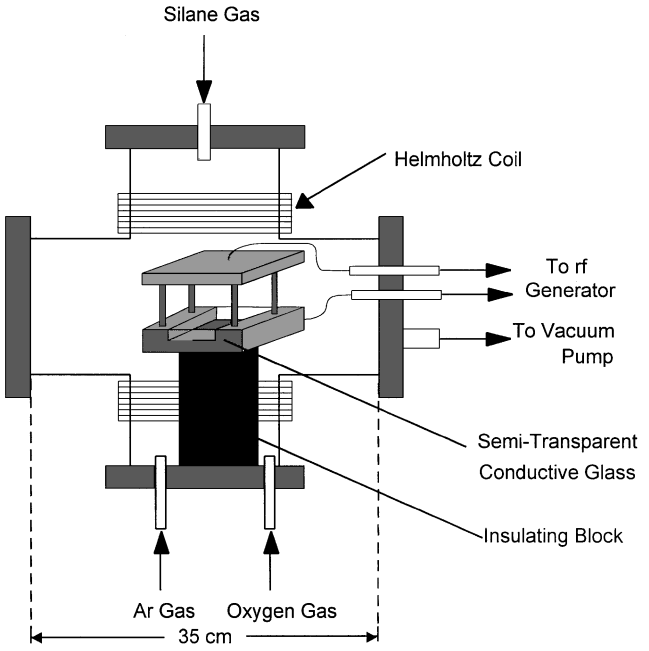

FIG. 1. The experimental setup used for dusty plasma Coulomb crystal generation.

hexagonal crystallites. Typical grains had an irregular rodlike shape of 100–140 μm length and 40–60 μm diameter.

The Ar pressure was raised to 150 mTorr at the end of the grain growth cycle. A 20 mW 640 nm diode laser was directed into the electrode groove for the observation of the grains. The dust grains condense into a geometric pattern a few minutes after the increase in Ar pressure. Top view images (with the help of a mirror held at 45° to the plane of the electrode) and side view images (through the conductive ITO coated glass plate) were taken with a charge coupled device camera and recorded on magnetic tape for analysis.

The lattice structure of the plasma crystal was studied as a function of forward rf power. Top view and side view images are shown in Figs. 3(a) and 3(b), respectively. Figure 3(a) is a top view of a typical hexagonal array formed at low forward rf powers below 2 W. As the power is increased the crystal loses its horizontal structure and breaks up into distinct columns of grains as shown in Fig. 3(b). The bottom of the electrode groove corresponds to the horizontal bright streak (from laser light scattering) at the bottom of the picture. The left (right) edge of the picture corresponds to the center (right sidewall) of the groove. The columns were observed to be robust, moving and interacting as single entities. Collisions between columns appear to be elastic and repulsive. This points to a screened repulsive interaction between columns. The robustness of the column suggests a strong attractive coupling between the grains of the column. More insight can be gained by noting the orientation of the columns in Fig. 3(b). While

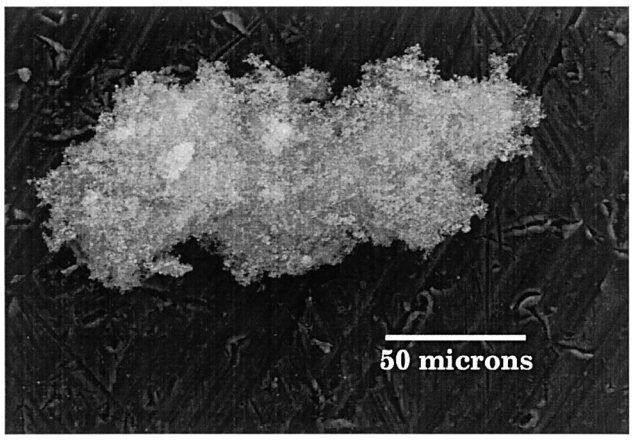

FIG. 2. Scanning electron micrograph of a dust grain formed during the growth process.

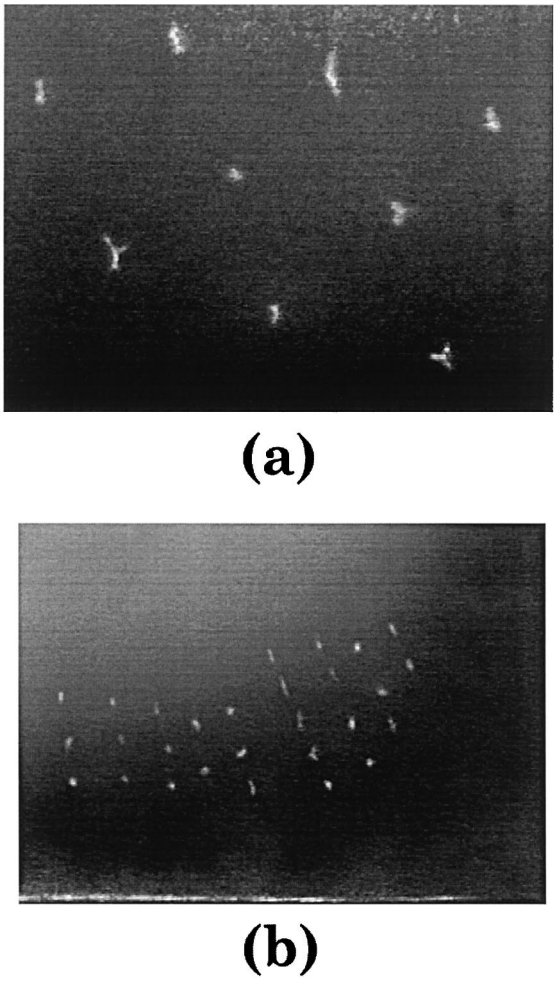

FIG. 3. (a) Top view of hexagonal array formed at forward rf powers below 2 W. (b) Side view image of the Coulomb crystal at large forward rf power taken through the transparent front electrode. The left (right) edge of the picture corresponds to the center (right sidewall) of the groove. The bright streak across the bottom of the picture corresponds to the groove bottom.

the columns near the center of the groove (left of picture) are vertical, those near the sidewall (right of picture) are tilted, with the tilt increasing with decreasing distance to the sidewall. The columns thus appear to be oriented parallel to the sheath electric field. The intergrain spacing along the columns as a function of the forward rf power is shown in Fig. 4. The thermal energy of the dust grains results in a distribution of intergrain spacings. The solid square represents the average spacing measured, and the limits on the error bar correspond to the maximum and minimum spacing measured at a given forward rf power.

The plasma temperature and density were measured using a Langmuir type single probe. A 0.5 mm diameter tantalum wire in a 0.63 cm ceramic sleeve was used. A 3 mm long exposed section of the probe was placed 1 cm above the bottom electrode. As dust contaminated the probe the measurements were done in a dust-free plasma at the same Ar pressure. The temperature of the plasma was calculated from the slopes of the I-V characteristics near the zero-current point [17]. The electron temperature (T_e) so derived is plotted along the left axis in Fig. 5 (dark squares). The range of temperatures shown by the error bars correspond to measurements ± 2 V around the zero-current point. T_e is seen to increase until 4 W rf forward power and thereafter saturate around 6 eV.

The ion saturation current was used to calculate the plasma density n [17], which is plotted as open circles along the right axis in Fig. 5. The error bars correspond to the error limits in the measurement of T_e. The density is observed to increase with increasing rf power. The debye length (λ_D) given by $\lambda_D = (T_e/4\pi ne^2)^{1/2}$ corresponding to the measured temperatures and electron densities decreases from 0.8 to 0.4 mm for forward rf powers between 1 and 10 W, respectively. This corresponds well to the decrease of intergrain spacing (Fig. 4), consistent with the assumption that the screened monopole Coulomb interaction plays a dominant role in the intergrain spacing.

We use a phenomenological model that appears to be consistent with the observations. From the experimental observations, there appear to be at least four main interactions that affect the formation of the Coulomb crystal with large grains of radius ~ 50 μm. These include (1) the electrostatic force due to the sheath electric field in the groove, (2) gravity, (3) the screened monopole repulsive interaction between the negatively charged grains, and (4) an attractive electric-field-induced dipole interaction (the ion drag force is much smaller, and is neglected). Foremost, the grains are levitated inside the electrode groove by the electrostatic force due to the sheath electric field E_0. Thus $eZ_dE_0 = m_dg$, where m_d is the dust mass [$m_d = (4\pi/3)\rho_d a^3$, where a is the grain radius and ρ_d is the grain mass density] and g is the acceleration due to gravity. Also $-eZ_d \sim a\phi_s$ for a negatively charged "isolated" grain (here ϕ_s is the grain surface potential). The sheath electric field can induce a polarization on the dust grains with a dipole moment P ($= E_0a^3$). The attractive dipole-dipole force between aligned dipoles separated by a distance d, taking into account screening by the background plasma, is given by [16]

$$F_{dd} = \frac{6P^2}{d^4}\left(1 + x + \frac{1}{2}x^2 + \frac{1}{6}x^3\right)\exp(-x), \quad (1)$$

where $x = d/\lambda_D$. Comparing this force with the screened monopole repulsion between the negatively charged dust grains given by

$$F_{mm} = \frac{Z_d^2e^2}{d^2}(1 + x)\exp(-x), \quad (2)$$

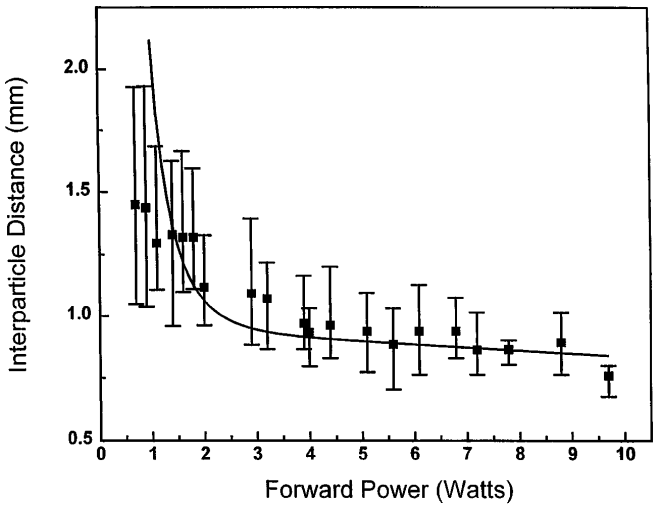

FIG. 4. The intergrain spacing d along the columns measured as a function of the forward rf power. The solid line is the predicted behavior of the phenomenological model with $x = 0$ for spherical grains of radius $a \approx 64$ μm.

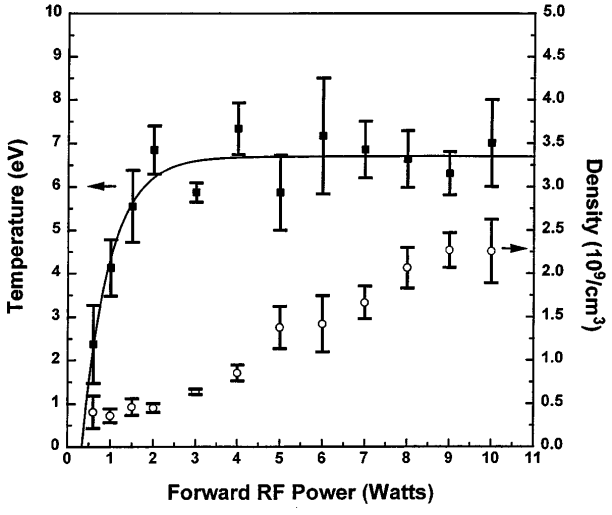

FIG. 5. The average plasma electron temperature (left axis) as dark squares and density (right axis) as open circles plotted as function of the forward rf power. The solid line is a best fit to the temperature data.

we estimate that $F_{dd}/F_{mm} \sim 6 \times 10^{-6}(a/d)^2 a^6 \phi_s^{-4}$, neglecting screening (here a and d are in microns, ϕ_s is in volts, and $\rho_d = 2.6\,\mathrm{g/cm^3}$). Thus F_{dd}/F_{mm} scales strongly with grain radius within our approximation and can be of order one in our case.

Balancing $F_{mm} = F_{dd}$ gives a rough equilibrium intergrain lattice spacing d for given plasma conditions represented by plasma (electron) temperature T_e (assuming $e|\phi_s| \sim T_e$) and plasma density n. This equilibrium spacing d derived from the above model is plotted as a function of the forward rf power as a solid line in Fig. 4. The values of T_e from the best fit curve of Fig. 5 were used. When screening is neglected (i.e., $x = 0$) the best fit corresponds to spherical grains of radius $a \approx 64\ \mu$m. If one includes screening, while noting that $x \approx 2$ for the entire range of rf power, then $a \approx 58\ \mu$m for the best fit. In both cases the porosity of the grains was neglected, i.e., $\rho_d = 2.6\ \mathrm{g/cm^{-3}}$. These values for the grain radius are consistent with the measured values (see Fig. 2). There is good agreement between the dipole-dipole interaction model and the observed dependence of the intergrain spacing with forward rf power. The grain dipole moment would lead to the observed orientation of the columns parallel to the sheath electric field.

We note that the electric-field-induced dipole interaction has been discussed in relation to dust plasma crystals [16] and to lattices of colloids in dilute suspension (e.g., [18–20]). We also note that other mechanisms for attractive interactions between grains in Coulomb crystals have been suggested. For example, the asymmetry of charge between the leading and trailing hemispheres of a dielectric grain in a flowing plasma can lead to a dipole moment of the grains, and this may lead to an attractive dipole-dipole force [21,22]. It has also been suggested that an attractive force between grains may arise from polarization of the Debye sheath around the grain by an external electric [23]. Another suggestion involves the focusing of ions flowing in the sheath due to deflection of ion orbits by the highly negatively charged grains leading to an attractive force [13]. Yet another suggestion involves wake potential effects in a plasma [14,15], which result in an attractive force between grains in the direction of flow. These suggestions have yet to be tested and may not even be mutually exclusive with one another or with the model proposed in the present paper.

In conclusion, we have measured the lattice structure and intergrain spacing of Coulomb crystals formed in rectangular conductive grooves as a function of plasma temperature and density. From the dynamics of the grains, the Coulomb crystal appears to be made of mutually repulsive columns of grains oriented along the sheath electric field and confined by the walls of the electrode groove. The main features of our experiment can be explained by a phenomenological model where the intergrain coupling along the column is determined by a balance between an attractive electric-field-induced dipole-dipole and a repulsive monopole interaction between the charged grains.

This work was supported at UCR by AFOSR Grant No. F49620-96-1-00113 and at UCSD by AFOSR Grant No. F49620-95-1-0293, NSF Grant No. ATM-9420627, and DOE Grant No. DE-FG03-97ER54444. The authors acknowledge help from J. Goodrich in the preparation of this manuscript.

*Author to whom correspondence should be addressed. Electronic address: umar.mohideen@ucr.edu

[1] E. C. Whipple, Jr., Rep. Prog. Phys. **44**, 1197 (1981).
[2] C. K. Goertz, Rev. Geophys. **27**, 271 (1989).
[3] D. A. Mendis and M. Rosenberg, Annu. Rev. Astron. Astrophys. **32**, 419 (1994).
[4] M. Horanyi, Annu. Rev. Astron. Astrophys. **34**, 383 (1996).
[5] T. W. Hartquist, W. Pilipp, and O. Havnes, Astrophys. Space Sci. **246**, 243 (1997).
[6] G. S. Selwyn, Jpn. J. Appl. Phys. **32**, 3068 (1993).
[7] A. Bouchele, Phys. World **6**, 47 (1993).
[8] H. Thomas, G. E. Morfill, V. Demmel, J. Goree, B. Feuerbacher, and D. Mohlmann, Phys. Rev. Lett. **73**, 652 (1994).
[9] J. H. Chu and Lin I, Physica (Amsterdam) **205A**, 183 (1994); Phys. Rev. Lett. **72**, 4009 (1994).
[10] Y. Hayashi and K. Tachibana, Jpn. J. Appl. Phys. **33**, L814 (1994).
[11] A. Melzer, T. Trottenberg, and A. Piel, Phys. Lett A **191**, 301 (1994).
[12] H. Ikezi, Phys. Fluids **29**, 1974 (1986).
[13] F. Melandso and J. Goree, J. Vac. Sci. Technol. A **14**, 511 (1996).
[14] S. V. Vladimirov and M. Nambu, Phys. Rev. E **52**, 2172 (1995).
[15] M. Nambu, S. V. Vladimirov, and P. K. Shukla, Phys. Lett. A **203**, 40 (1995).
[16] H. C. Lee, D. Y. Chen, and R. Rosenstein, Phys. Rev. E **56**, 4596 (1997).
[17] I. H. Hutchinson, *The Principles of Plasma Diagnostics* (Cambridge University Press, New York, 1987).
[18] R. E. Kusner, J. A. Mann, J. Kerins, and A. J. Dahm, Phys. Rev. Lett. **73**, 3113 (1994).
[19] Q. Lei, X. Lei, C. Zhou, and N. Ming, Phys. Rev. E **51**, 1586 (1995).
[20] P. A. Adriani and A. P. Gast, Faraday Discuss. Chem. Soc. **90**, 17 (1990).
[21] G. Lapenta, Phys. Rev. Lett. **75**, 4409 (1995).
[22] J. W. Manweiler, T. P. Armstrong, and T. E. Cravens, in *The Physics of Dusty Plasmas*, edited by P. K. Shukla *et al.* (World Scientific, Singapore, 1996), p. 22.
[23] S. Hamaguchi and R. T. Farouki, Phys. Rev. E **49**, 4430 (1994).